NACA

RESEARCH MEMORANDUM

THE EFFECT OF FLUID INJECTION ON THE COMPRESSIBLE TURBULENT BOUNDARY LAYER - PRELIMINARY TESTS ON TRANSPIRATION COOLING OF A FLAT PLATE AT M = 2.7 WITH AIR AS THE INJECTED GAS

By Morris W. Rubesin, Constantine C. Pappas,
and Arthur F. Okuno

Ames Aeronautical Laboratory
Moffett Field, Calif.

NATIONAL ADVISORY COMMITTEE
FOR AERONAUTICS
WASHINGTON

December 21, 1955
Declassified September 13, 1957

NATIONAL ADVISORY COMMITTEE FOR AERONAUTICS

RESEARCH MEMORANDUM

THE EFFECT OF FLUID INJECTION ON THE COMPRESSIBLE TURBULENT BOUNDARY LAYER - PRELIMINARY TESTS ON TRANSPIRATION COOLING OF A FLAT PLATE AT M = 2.7 WITH AIR AS THE INJECTED GAS

By Morris W. Rubesin, Constantine C. Pappas, and Arthur F. Okuno

SUMMARY

Local values of heat-transfer rate and temperature-recovery factor, obtained on a transpiration-cooled flat plate, are presented. Air was injected into a turbulent boundary layer at several rates of flow through a porous flat plate oriented parallel to an air stream. Surface temperatures were maintained near recovery temperature. The Mach number was 2.7 and the Reynolds number range was 1.5×10^6 to 7.0×10^6. The results for nearly uniform injection show: (1) The ratio of local Stanton number with injection to that with zero injection decreases appreciably with increased injection rate and this decrease is greater at the higher Reynolds numbers. The decrease is comparable to the predicted theoretical values. (2) The local temperature-recovery factor decreases with increasing injection rate at a given Reynolds number and the rate of decrease is greater at the higher Reynolds numbers. These effects are not predicted by the theory. (3) The transpiration cooling process requires considerably less coolant than conventional heat exchangers to maintain a given cooled surface temperature, especially for high cooling loads.

INTRODUCTION

A comparison of the effectiveness of surface cooling methods (ref. 1) has indicated that a transpiration cooling system offers promise as a possible solution of the aerodynamic heating problem associated with high-speed flight. A transpiration cooling system for an aircraft surface is defined as one in which the coolant passes from within the interior of the aircraft through a porous skin and then out into the boundary layer on the surface. The effectiveness of this system is due to two conditions:

(1) The large wetted area within the multitude of pores in the skin results in a high heat exchange between the coolant and the skin, and (2) the injection of the coolant into the boundary layer affects the boundary layer so as to reduce the amount of heat entering the aircraft. The second of these conditions has been predicted by theory, references 2 through 6, and has been observed experimentally in low-speed tests (ref. 7) and at a Mach number of 2 (ref. 8). The subject of the present investigation is an experimental examination of this second condition under high-speed conditions; namely, an experimental study of the effectiveness of coolant injection in reducing the heat transferred to the surface of aircraft by aerodynamic heating.

Examples of the magnitudes of the reductions in heat transfer by coolant injection as predicted by theory are shown in figure 1 (taken from ref. 9). It is noted in this figure that a simultaneous reduction of skin friction by the injection of fluid occurs. The ordinate of figure 1 represents the ratios of the skin friction and heat-transfer coefficients to their values corresponding to zero injection. The abscissa is a dimensionless grouping containing the mass flow of the injected gas normal to the surface. It is apparent that the theoretically predicted reductions associated with injection can be extremely large.

The theoretical bases for the laminar boundary-layer results are fairly sound. This, however, is not true for the turbulent boundary-layer theories, references 5 and 6. The theories dealing with the compressible, turbulent boundary layer are essentially weak in that their final answers are largely determined by arbitrary assumptions concerning the structure of the turbulent boundary layer. (For a discussion of this point, see ref. 6.) In view of this, the present tests are confined to the turbulent boundary layer. Additional reasons for stressing the turbulent boundary layer are (1) that it is believed that fluid injection tends to destabilize laminar boundary layers and cause transition to turbulent flow making the turbulent boundary layer more probable under conditions of injection and (2) that under comparable conditions of Reynolds number and temperature potential, aerodynamic heating is more severe for a turbulent boundary layer.

The present tests were made to determine the effect of injection rate on the local heat transferred to a cooled flat plate oriented parallel to an air stream. The Mach number was 2.7 and the Reynolds number range was 1.5×10^6 to 7×10^6. The boundary layer was tripped to assure turbulent flow. Cooling air was injected through the porous surface of the plate with no attempt made to adjust the distribution of injection rate along the plate. The temperature rise of the coolant air as it passed from the interior on through the surface of the plate provided a measure of the heat transferred to the plate. Comparison was then made with the theoretical results of reference 6 in order to assess the value of the theories as means for extrapolating to conditions not covered by the tests.

SYMBOLS

c	specific heat per unit weight of solid material of porous plate
c_f	local skin-friction coefficient
c_p	specific heat per unit mass at constant pressure of gas
F	dimensionless mass-flow rate normal to surface, $\frac{\rho_w v_w}{\rho_\infty u_\infty}$
h	heat-transfer coefficient
k	thermal conductivity of porous solid
M	Mach number
Pr	Prandtl number
p_t	wind-tunnel stagnation pressure
q	local heat-transfer rate per unit area
R_x	Reynolds number, $\frac{u_\infty \rho_\infty x}{\mu_\infty}$
St	Stanton number, $\frac{h}{\rho_\infty u_\infty c_p}$
t	temperature
T	absolute temperature
u	velocity component parallel to surface
v	velocity component normal to surface
w	thickness of porous plate
x	coordinate parallel to streamwise direction measured from leading edge
y	coordinate parallel to surface of plate and normal to stream direction
z	coordinate perpendicular to surface of the plate measured from inner face
η_r	temperature recovery factor

ρ	mass density of gas
μ	viscosity of gas

Subscripts

c	initial condition of coolant
o	zero injection condition
r	recovery condition or zero heat-transfer condition
w	condition at surface
∞	condition at outer edge of boundary layer
1,2,3,4	position designation of thermocouples

Superscripts

$(\bar{\ })$	temperature function defined in equation (A7)
*	temperature function defined in equation (A7)

DESCRIPTION OF EXPERIMENT

Wind Tunnel

These tests were made in the Ames 6-inch heat-transfer wind tunnel described in reference 10. The tunnel is continuous-operating and has controllable stagnation pressure and temperature in the ranges of 5 to 55 pounds per square inch absolute and 80° to 160° F, respectively. The nozzle is made of a single curved wall and flat opposite and side walls. The tunnel specific humidity was maintained less than 0.0003 pound of water per pound of dry air.

Flat-Plate Model

The model consisted of a hollow chamber with a porous plate as the top surface. The model was mounted on a hollow vertical sting through which the coolant air was introduced. The heat transferred to the model

was measured with thermocouples by determining the temperature rise of the coolant as it passed from underneath the porous wall to its outer surface. The simplicity of the model did not allow control of the distributions along the model of surface temperature or injection rate. This was not believed to be a serious shortcoming because the expected effect of transpiration on heat transfer is large and an experiment of limited accuracy would still provide useful results.

The test surface of the flat-plate model was made of a porous, sintered, powdered, stainless-steel sheet, approximately 1/8 inch thick, similar to specimen 5 of reference 11, and was mounted in the hollow steel body as shown in figure 2(a). The steel body was supported by a hollow, vertical strut through which the transpiration air enters. Bakelite sheets were bonded to the flat-plate steel body and vertical strut to provide heat insulation for the porous surface and the transpiration air. The flat-plate body completely spanned the wind-tunnel section and seals were used to prevent air leakage from the lower to the upper side of the plate body. The upstream end of the model was chamfered to form an angle of 10°, and the leading edge was rounded to a radius of about 0.002 inch to avoid feathering. The effective porous area of 0.316 square foot started 1-7/8 inches back from the leading edge and extended for 10-7/8 inches along the plate with a width of 4-3/16 inches.

A boundary-layer trip, consisting of a 1/2-inch-wide strip of 5/0 garnet paper, was cemented to the plate 1/8 inch back from the 10° wedge leading edge. This trip was approximately 0.010 inch high.

Thermocouples, made from number 36-gage Nichrome V - Advance wire with enamel insulation, were used for the heat-transfer instrumentation and were located at nine stations along the plate at 1-inch intervals, starting at $x = 3\text{-}7/8$ inches from the plate leading edge. The thermocouples were installed as shown in figure 2(b). Each type of installation was designed to eliminate conduction errors as much as possible. Along the center line, thermocouples were placed at each station to measure the temperature of the outer porous surface (location 1) and the temperature of the transpiration air (location 3) before entering the porous material. Thermocouples were located at alternate stations on the center line to measure the inner porous-surface temperature (location 2); and on two lines 1 inch off the center line to measure the outer porous-surface temperature (location 1). Typical Nichrome V - Advance wire thermocouples were calibrated with a standard NBS thermocouple over the temperature range encountered in these tests. Estimated accuracy of model temperature readings was $\pm 0.5^{\circ}$ F.

The transpiration air was dried and cooled before entering the model, and was metered with two different capacity rotometers placed ahead of the cooling unit. The relative porosity of the plate was determined in calibration tests and is shown in figure 3 expressed as the ratio of local flow rate to the average flow rate over the plate. Porosity measurements

were made before and after the tests for conditions near the minimum and maximum flow rates of 72 and 540 pounds per hour per square foot, respectively. The porosity calibration was made using an air-supply element consisting of two concentric chambers that are sealed with O-rings from each other and the surroundings when the element is pressed against the porous surface. The outer chamber was maintained at the same pressure as the inner chamber and acted as a guard unit to assure unidirectional flow in the porous material beneath the center chamber. The diameter of the center chamber was 1.03 inches. Only the air in the center chamber was metered.

Static pressures were measured with a static-pressure probe made of 0.100-inch-outside-diameter stainless-steel tubing. This tube had an ogival head with four equally spaced orifices, 0.0135 inch in diameter, located at a cross section 0.79 inch from the tip.

TEST CONDITIONS AND PROCEDURE

The heat-transfer tests were conducted at an average Mach number of 2.7 over the range of Reynolds numbers from 1.5 million to 7 million and at average dimensionless transpiration rates of $F = 0.001$, 0.002, and 0.003. The wind-tunnel stagnation temperature was maintained at approximately 150° F. Transpiration air was admitted to the porous plate at two different temperatures at each injection rate to enable the determination of the heat-transfer coefficients and the recovery factors (see "Reduction of Data" section).

During the actual heat-transfer tests, time-steady conditions of wind-tunnel stagnation temperature and pressure, transpiration air temperature and rate of flow, and model temperatures were established before the various model and transpiration air temperatures were recorded.

Only the heat-transfer data obtained in the fully developed turbulent flow region from stations 4 to 8 (x = 6-7/8 to 10-7/8 inches), inclusive, are presented in this report. This region was bounded at the upstream position by the end of transition as indicated by boundary-layer surveys and was limited at the downstream position by the weak reflected shock waves emanating from the plate leading edge.

The local free-stream Mach number distribution along the plate was obtained for all heat-transfer runs from measurements of local static pressure and tunnel stagnation pressure for positions from 4 to 11-3/4 inches, inclusive, from the leading edge. These results agree within ±1 percent of the Mach number determined from the values of local free-stream static and impact pressures. Typical Mach number distributions up to 11 inches are presented in figure 4. The maximum variation of the Mach number was ±2 percent of the mean free-stream Mach number for all test

conditions. Because of a tunnel blockage problem with the static-pressure survey mechanism in place, complete data were not obtained at x = 10 inches and x = 11 inches.

REDUCTION OF DATA

Basic Heat Balance

The heat-transfer rates to the plate were determined using an expression resulting from a heat balance on an element of the porous-plate surface. Details of the heat balance are presented in Appendix A. The result of the heat-balance analysis is given by

$$h(t_r - t_w) = \rho_w v_w c_p (t_w - t_c) - kw \left(\frac{t_{w1} + t_{w2} + t_{w3} + t_{w4} - 4t_w}{\Delta^2} \right) \quad (1)$$

The term on the left side of equation (1) represents the heat flow rate per unit surface area into the porous element. The first term on the right side of the equation represents the rate of heat gained by the coolant as it passes from beneath the porous element where it has its original temperature, t_c, to its final temperature, t_w, corresponding to the outer surface temperature of the element. The second term on the right side represents the rate of heat conduction into the element in terms of finite differences. The terms t_{w1}, t_{w2}, t_{w3}, and t_{w4} represent the temperatures on the four sides of the point in question having the temperature t_w. The Δ represents the distance chordwise and spanwise between adjacent thermocouples, which was 1 inch in all cases. For x = 4-7/8, 6-7/8, 8-7/8, and 10-7/8 inches, there were no spanwise thermocouples. These temperatures were interpolated from the side values of the other stations. The thermal conductivity of the porous material was found in the manner described in Appendix A. Thus, the entire right side of equation (1) can be evaluated directly from the data. The second term on the right side was found to be less than 10 percent of the first.

Evaluation of h and t_r

If the right side of equation (1) is replaced by the symbol q, the equation becomes

$$q = h(t_r - t_w) \quad (2)$$

For small changes of surface temperature with respect to its absolute value, both the heat-transfer coefficient and the recovery temperature will be essentially independent of surface temperature level. Thus, if the coolant temperature level is changed while the wind-tunnel Reynolds

and Mach numbers remain constant, the only terms in equation (2) that will change are q and t_w. Because of the linear character of equation (2), two (or more) settings of the coolant temperature level provide sufficient information to calculate both h and t_r at each station. Because of the preliminary nature of these tests, data were obtained at only two coolant temperatures corresponding to each test condition. From the two sets of data, both h and t_r were found conveniently from a plot similar to that shown in the following sketch.

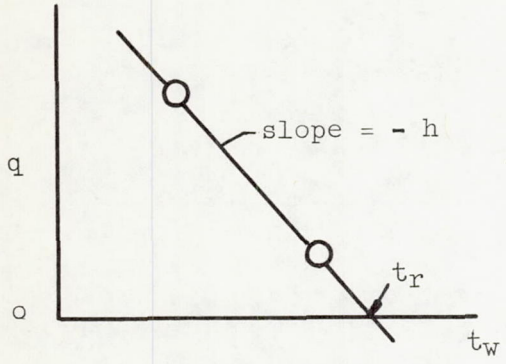

Each indicated data point was an average of at least five runs. An occasional check run taken at different temperatures indicated that reproducibility in heat transfer was generally within 5 percent with an occasional larger variation. Since one of the data points was in all cases near recovery temperature, the error in evaluating the recovery factor was minimized.

For the zero transpiration condition the recovery temperature was the measured wall temperature. The conduction corrections were negligible for this condition.

Influence of Surface Temperature Distribution

The model had the advantage of simplicity of construction; however, it had the disadvantage of allowing the distributions (with x direction) of the air injection and the surface temperature to be uncontrolled along its surface. Before considering the test results in detail, it is important to discuss the influence of the lack of control of these factors on the heat-transfer data.

A typical surface temperature distribution along the porous plate is shown in figure 5. On comparison of this distribution with the temperature distribution of the coolant air beneath the plate surface, it is seen that the temperature of the porous plate is essentially governed by the temperature distribution of the coolant. The variation in temperature exhibited by the coolant is the result of heat addition to the air from the external surfaces of the vertical strut and the hollow flat-plate body. At the present, there is no experimental or theoretical information concerning the effect of variation of surface temperature on the heat transferred in a compressible turbulent boundary layer with or without air injection. It was necessary to use the incompressible turbulent boundary-layer theory of reference 12 to estimate the effect of the variable surface temperature. On this basis it was found that the surface temperature distributions

occurring in these tests (e.g., see fig. 5) would cause an increase of the local heat-transfer coefficient over that which would exist for a constant surface temperature. The magnitude of the increase ranged from an average of 13 percent at station 4 to 4 percent at station 8. At each station, a scatter in this increase of about ±2 percent about the mean occurred for the different pressure levels and injection rates. There were no particular trends with injection rate or pressure level. Since use of incompressible theory is questionable under conditions of compressible flow, no quantitative corrections were applied to the data.

Influence of Variation in Injection Rate

Control of the injection distribution over the surface of the plate was not attempted because of the complexities of model construction that would be introduced. The resulting variation of injection rate (see fig. 3) was produced by the inherent variation of porosity of the surface material and some clogging which occurred during the tests. This clogging occurred even though a filter was placed in the pipeline upstream of the model and caused the effective porosity of the surface to be time-dependent. Essentially then, the effective porosity distribution at any particular time was not known; however, it is believed to fall between the limits of the data shown in figure 3.

Examination of equation (1) and the method used for determining h and t_r revealed that the value of Stanton number was essentially proportional to the injection rate. In view of the uncertainty of the value of local injection rate at any given time, it was decided to use the average injection rate over the entire plate in the evaluation of the local Stanton number. This results in values of local Stanton number that are on an average about 7 percent lower than those computed using an arithmetic average of the data in figure 3 over the entire test region from $x = 6\text{-}7/8$ to 10-7/8 inches. The Stanton number presented in this report also ranges almost 30 percent lower and 10 percent greater than the values of Stanton number which could have been computed if the extreme variations of the injection-rate values within the test region had been used.

Influence of Mach Number Variation and Effective Starting Length

The Mach number distributions over the plate have been presented in figure 4 and show maximum variations of about ±2 percent. Estimations of the effect of these variations on local heat transfer reveal an expected influence of less than 2 percent which is well within the scatter of the data.

The effective starting position for the fully developed turbulent boundary layer for conditions with injection has been estimated from boundary-layer surveys made on the test plate in the region where the heat-transfer data have been obtained. The effective Reynolds number was found to be between 7 and 15 percent less than R_x for conditions with injection. It is estimated from the mean slope of the $St(R_x)$ data that the St values presented are on an average 4 percent high when plotted against the physical R_x.

Estimation of Over-All Accuracy

In the above discussion it was estimated that the measured Stanton number is, on the average, about 8 percent greater than would have existed on a plate with constant surface temperature. Further, it was shown that the measured Stanton number is, on the average, about 7 percent lower than one computed using local injection rates. These effects are, in general, compensating. Also the expected influence of the Mach number variation and the effective starting length considerations would tend to increase the Stanton number less than 2 percent and an average of 4 percent, respectively. It is concluded then, that the Stanton numbers presented in this report when correlated with respect to physical Reynolds number correspond to a flat plate with constant surface temperature and uniform injection with a consistent positive error of about 6 percent and an estimated uncertainty of less than ±20 percent.

Discussion of Results

The results of Stanton number plotted against Reynolds number are presented in figure 6. The data are compared with a line representing the relationship between Stanton number and Reynolds number for zero injection. This line was determined by starting with the well-known Colburn equation which applies to low-speed flow and then adjusting the values of Stanton number to correspond to conditions for Mach number of 2.7 by the empirical curve of reference 13. This curve applies to the case where the surface temperature is approximately equal to the recovery temperature, which prevailed during the present tests. The primary result shown by these data is that there is an appreciable decrease in local Stanton number with injection as compared with the zero injection case. Also, the variation of local Stanton number with R_x tends to increase in negative slope with increased injection rate as is expected from theory for uniform injection (ref. 6).

The ratio of Stanton number, St, with transpiration compared with that for no transpiration, St_o, is presented in figure 7 as a function of transpiration parameter F. This figure results from cross-plotting

figure 6. The two curves shown represent the theory of reference 6[1] evaluated for uniform injection and for the Reynolds numbers at the upper and lower limits of these tests. The variation in the experimental values of St/St_o is partly due to the inherent experimental uncertainties but also includes the effect of the Reynolds number change between positions. The large reduction in Stanton number with injection is evident. The average of the local values of St/St_o from x = 6-7/8 to 10-7/8 inches at each F value is presented as a heavy bar in figure 7. This average variation of St/St_o with F may be considered as a useful result for application to design. Reductions in Stanton number of 55 percent occur at F = 0.003. The measured reduction in Stanton number is comparable but slightly less than the theoretically predicted reductions.

It is desirable to obtain the zero transpiration Stanton numbers from the present tests for comparison with the modified Colburn equation which has been used to define the zero transpiration heat-transfer values presented previously. Normally, the St_o value would be obtained by measuring the heat-transfer rate at lower and lower transpiration rates with the measured Stanton numbers converging to the F = 0 value. For this test, however, it was not possible to measure the heat transfer at lower transpiration rates than F = 0.001 because the temperature gradient normal to the surface in the transpiration air beneath the plate extended beyond the position of the thermocouples used for determining the air temperature. These thermocouples were not located farther away from the porous surface because of the space limitation and because it was desired to have the thermocouples placed in the region where the air flowed normal to the surface. Since no experimental data were obtained for $F < 0.001$, the theory of reference 6 was used as a guide to extrapolate the experimental Stanton numbers to the zero transpiration condition (see Appendix B for details). The extrapolated experimental values are compared with the modified Colburn equation in figure 8. On an average the extrapolated St_o values are within 10 percent of the modified Colburn equation. This difference is not sufficiently large to alter appreciably the results shown in figure 7.

The effects of injecting air into the boundary layer on the temperature recovery factor are clearly brought out in figure 9. The recovery factors for the zero transpiration condition were determined in this investigation and agree very well with values from other experiments (see ref. 13). The recovery factor decreases from the zero transpiration value of 0.89 to a value of 0.70 for F = 0.003 at $R_x = 6 \times 10^6$. These

---

[1]The theory of reference 5 cannot be used conveniently in this comparison since numerical results of this theory at the conditions of the present tests can only be obtained through extensive numerical integrations. Previous comparisons of the theories of references 5 and 6 have indicated agreement between the theories, with differences less than those produced by reasonable changes in the assumptions imposed. Thus, conclusions arrived at concerning the theory of reference 6 should apply equally to the theory of reference 5.

appreciable variations are not indicated from the theoretical predictions of references 5 and 6, although it might be noted that laminar boundary-layer theory predicts a dropoff of laminar recovery factor with injection. A cross plot (fig. 10) of figure 9 shows the decrease in recovery factor as a function of the injection rate at the extremes of the test Reynolds number range.

The effectiveness of the transpiration cooling process may be seen in figure 11, from the theoretical curves of reference 6 and the experimental data, where the wall temperature parameter, $(t_w - t_c)/(t_{r_o} - t_c)$, is presented as a function of the transpiration-rate parameter, F, for Stanton number invariant with transpiration rate and for Stanton number varying with transpiration rate. The curve with Stanton number ($St = St_o$) invariant with F represents the case of a 100-percent effective heat exchanger at a given initial coolant temperature t_c and flow rate F acting on the inside of a nonporous surface. The curve with Stanton number varying with F represents the transpiration heat-transfer process. The comparative effectiveness of transpiration may be seen for the condition where an outer surface temperature t_w is specified on an aircraft by equipment and structural considerations during a given flight path. With t_c and t_{r_o} given and $(t_w - t_c)/(t_{r_o} - t_c)$ specified to a value of 0.3, for example, the conventional 100-percent effective heat-exchanger system would require 1.7 times the coolant flow of a transpiration system. For high cooling loads where the wall-temperature parameter is small, the conventional heat-exchanger system requires several times the coolant flow of a transpiration system.

The wall-temperature parameter obtained from experimental measurements for the R_x range of 2×10^6 to 6.8×10^6 is compared with the theory of reference 6 in figure 11. The test results are consistently lower than the theoretical predictions; whereas the experimental St values shown in figure 7 are higher than theory predicts. Note, however, that the wall-temperature parameter

$$\frac{t_w - t_c}{t_{r_o} - t_c} = \frac{t_r - t_c}{t_{r_o} - t_c} \frac{St}{F + St}$$

may be expressed as a product of two factors, one depending on the recovery temperature, the other depending on the Stanton number. The term $(t_r - t_c)/(t_{r_o} - t_c)$ theoretically has a value near unity and is essentially invariant with F; however, the experimental recovery temperature decreases with increased transpiration and this effect causes a decrease in wall-temperature parameter below the theoretical predictions.

The measured temperature ratios $(t_w - t_c)/(t_{r_o} - t_c)$ of reference 8, obtained on an 8° porous cone at $M_\infty = 2.0$ with nitrogen as the transpired gas, are compared to the present results (dashed curve) in figure 12. The dashed curve is the predicted temperature ratio corresponding to the test conditions of reference 8 and is based on the recovery factor and

St/St_o vs. F results of the present tests modified to $M_\infty = 2.0$. The agreement is good except for the result at the highest injection rate of F = 0.00135; however, this comparison is somewhat inconclusive because it does not extend to sufficiently large F values.

CONCLUDING REMARKS

The preliminary tests presented provide useful information to guide a future experimental test program and also provide information for assessing the worth of using theoretical predictions for design purposes.

These results show primarily that transpiration cooling in a turbulent boundary layer at M = 2.7 has marked effects on the heat transfer and the recovery temperature for nearly uniform air injection along the plate; specifically,

1. The ratio of local Stanton number with transpiration to that with zero transpiration decreases appreciably with increased injection rate; reductions as much as 55 percent were achieved. The decrease is comparable to, although less than, the theoretical predictions of references 5 and 6.

2. The local temperature recovery factor, η_r, decreases with increasing injection rate at a given Reynolds number, and the rate of decrease is greater at the higher Reynolds numbers. Reduction to $\eta_r = 0.7$ was attained.

3. The wall-temperature parameter $(t_w - t_c)/(t_{r_o} - t_c)$, representing the degree of cooling achieved by the surface, decreases with injection rate more than is predicted by the theory of reference 6. The transpiration cooling process requires considerably less coolant flow than conventional heat exchangers to maintain a given cooled surface temperature, especially for high cooling requirements.

Ames Aeronautical Laboratory
National Advisory Committee for Aeronautics
Moffett Field, Calif., Sept. 19, 1955

APPENDIX A

HEAT BALANCE

Consider the element within the porous surface shown in the following sketch:

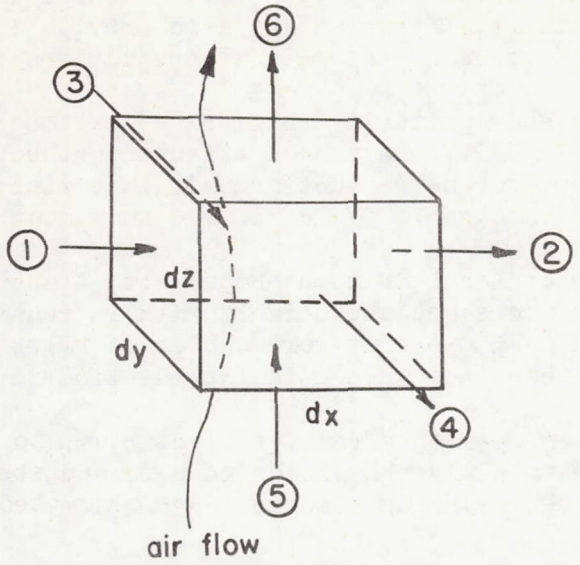

In this system, there are two factors which govern the time steady-state heat balance. There is the heat conducted by the solid material of the porous plate and there is the heat picked up by the cooling air as it passes through the element. It is assumed that the temperature of the air and solid material at a point are the same because of the small dimensions of the pores in the solid material. Calculations based on the methods of reference 14 for the material used in these tests confirmed this assumption. Subject to these assumptions, the heat balance is as follows:

Heat conducted in x direction

In

$$(1) = - k \, dy \, dz \, \frac{\partial t}{\partial x}$$

Out

$$(2) = - k \, dy \, dz \, \frac{\partial t}{\partial x} - k \, dy \, dz \, \frac{\partial^2 t}{\partial x^2} \, dx$$

Note that the thermal conductivity of the solid is assumed to be constant. The net heat conducted into the element in the x direction is then ①-②, or $k\,dx\,dy\,dz(\partial^2 t/\partial x^2)$. Similarly, the net heat conducted into the element in the y and z directions is $k\,dx\,dy\,dz\,(\partial^2 t/\partial y^2)$ and $k\,dx\,dy\,dz\,(\partial^2 t/\partial z^2)$. The heat absorbed by the air in passing through the element in the z direction is the rate of mass flow times the specific heat times the change in temperature which equals $\rho_w v_w\,dx\,dy\,c_p(\partial t/\partial z)dz$. When the heat entering the element is equated to the heat absorbed, there results

$$k\left(\frac{\partial^2 t}{\partial x^2} + \frac{\partial^2 t}{\partial y^2} + \frac{\partial^2 t}{\partial z^2}\right) = \rho_w v_w c_p \frac{\partial t}{\partial z} \tag{A1}$$

Now the inner surface of the porous plate will not be, generally, at the initial temperature of the coolant. The coolant will pick up some heat as it flows toward the porous plate. Since this heat must come from the porous plate, a boundary condition at the inner surface of the porous plate ($z = 0$) is

$$k\left(\frac{\partial t}{\partial z}\right)_{z=0} = \rho_w v_w c_p (t_{z=0} - t_c) \tag{A2}$$

where the heat conducted out by the solid is equal to the heat gained by the coolant. At the outer surface of the porous plate ($z = w$), the heat entering the plate by convection equals that conducted in by the solid material

$$k\left(\frac{\partial t}{\partial z}\right)_{z=w} = h(t_r - t_w) \tag{A3}$$

Suppose equation (A1) is integrated with respect to z from $z = 0$ to $z = w$

$$k\int_0^w \left(\frac{\partial^2 t}{\partial x^2} + \frac{\partial^2 t}{\partial y^2}\right) dz + k\left(\frac{\partial t}{\partial z}\right)_{z=w} - k\left(\frac{\partial t}{\partial z}\right)_{z=0} = \rho_w v_w c_p (t_w - t_{z=0}) \tag{A4}$$

In this integration $\rho_w v_w$ is kept constant with z implying unidirectional flow through the plate. When equations (A2) and (A3) are substituted into equation (A4) there results

$$k\int_0^w \left(\frac{\partial^2 t}{\partial x^2} + \frac{\partial^2 t}{\partial y^2}\right) dz - \rho_w v_w c_p (t_{z=0} - t_c) + h(t_r - t_w) = \rho_w v_w c_p (t_w - t_{z=0}) \tag{A5}$$

or

$$h(t_r - t_w) = \rho_w v_w c_p (t_w - t_c) - k\int_0^w \left(\frac{\partial^2 t}{\partial x^2} + \frac{\partial^2 t}{\partial y^2}\right) dz \tag{A6}$$

Equation (A6) is the basic equation that allows evaluation of the heat transferred to the plate. In addition, it was not possible to instrument the porous surface in three dimensions so as to define the third term on the right of equation (A6) precisely. It can be assumed, and this was borne out experimentally, that

$$t \approx \bar{t}(x,y) + t^*(z) \tag{A7}$$

This means that at a given (x,y) position the temperature in any plane parallel to the surface within the porous plate differs from that at any other parallel plane by essentially a constant value no matter where the point is located. Typical temperature distributions on the porous plate and in the coolant air beneath the surface are shown in figure 5. These data reveal that the lower surface is about 2° F cooler than the upper surface in this case. The difference between the upper and lower surface is essentially constant over the plate, these differences varying by less than 1° F. This shows that the assumption represented by equation (A7) is fairly accurate. When equation (A7) is substituted into equation (A6), there results on integration

$$h(t_r - t_w) = \rho_w v_w c_p (t_w - t_c) - kw\left(\frac{\partial^2 \bar{t}}{\partial x^2} + \frac{\partial^2 \bar{t}}{\partial y^2}\right) \tag{A8}$$

As $\bar{t}$ is not a function of z we can replace it with t_w.

$$h(t_r - t_w) = \rho_w v_w c_p (t_w - t_c) - kw\left(\frac{\partial^2 t_w}{\partial x^2} + \frac{\partial^2 t_w}{\partial y^2}\right) \tag{A9}$$

Equation (A9) represents the fundamental expression used in these tests for evaluating h and tr. For numerical solution of this equation, the Laplacian was replaced by its first-order equivalent in terms of finite differences. This approximation is permissible because the conduction term is small (usually less than 10 percent) in comparison with the term representing the heat gained by the coolant and is only considered as a correction term. Thus, equation (A9) was replaced by

$$h(t_r - t_w) = \rho_w v_w c_p (t_w - t_c) - kw\left(\frac{t_{w1} + t_{w2} + t_{w3} + t_{w4} - 4t_w}{\Delta^2}\right) \tag{A10}$$

In equation (A10), t_{w1}, t_{w2}, t_{w3}, and t_{w4} represent the surface temperatures measured on the four sides of the point in question which has the temperature t_w. The Δ represents the distance chordwise and spanwise between adjacent thermocouples, which was 1 inch in all cases. For $x = 4\text{-}7/8$, $6\text{-}7/8$, $8\text{-}7/8$, and $10\text{-}7/8$ inches there were no spanwise thermocouples; however, these side temperatures were interpolated from the side values at $x = 3\text{-}7/8$, $5\text{-}7/8$, $7\text{-}7/8$, $9\text{-}7/8$, and $11\text{-}7/8$ inches.

With the known value of the thermal conductivity,[1] the entire right side of equation (A10) was evaluated from the data.

[1]The thermal conductivity was found to be 3.6 Btu per hour, $^{\circ}$F foot at 85° F. This was determined by comparison with a material of known conductivity by heating both specimens at one end and measuring the temperature distribution along each bar. The heat losses to the ambient air from the material of known conductivity were obtained, and this knowledge was sufficient to calculate the heat losses from the porous bar and finally the thermal conductivity of the porous material.

APPENDIX B

EXTRAPOLATION OF EXPERIMENTAL DATA TO ZERO TRANSPIRATION CONDITION

The experimental method used in these tests did not provide a means of measuring zero transpiration heat transfer. Since it is desirable to compare the heat-transfer data with previous experimental zero transpiration heat-transfer results, a method was devised to extrapolate the present St/St_o values to the zero transpiration case. It is noted from the theoretical St/St_o vs. F curves of figure 7 that a linear extrapolation using the St/St_o values at $F = 0.001$ and 0.002 is inadequate and that the curvature must be considered in the extrapolation to $F = 0$ to obtain the theoretical value of $St/St_o = 1$. The method adopted for the extrapolation of the experimental St/St_o data to the zero transpiration case was to extrapolate the experimental and theoretical St/St_o values at $F = 0.001$ and 0.002 linearly to $F = 0$ and to divide the experimental extrapolated value by the theoretical linearly extrapolated value to account for the theoretical curvature. A mathematical justification of this type of extrapolation may be seen from the following considerations. If St/St_o is denoted as $\alpha = \alpha(F)$ and subscripts 0, 1, and 2 refer to $F = 0$, 0.001, 0.002, respectively, and subscripts e and t refer to experiment and theory, the extrapolated experimental value may be written as

$$\alpha_{o_e} = \alpha_{o_e}' \frac{1}{\alpha_{o_t}'} = \alpha_{o_e}' \frac{\alpha_{o_t}}{\alpha_{o_t}'}$$

where $\alpha_{o_t} = 1$ and the primed values are the linearly extrapolated values to $F = 0$. Now, for the theoretical curves

$$\alpha_{o_t}' = \alpha_{1_t} - \left(\frac{\alpha_2 - \alpha_1}{F_2 - F_1}\right)_t F_1 \approx \left[\alpha_m - \left(\frac{d\alpha}{dF}\right)_m m\right]_t$$

where $F = m$ when $\left(\frac{d\alpha}{dF}\right)_m = \frac{\alpha_2 - \alpha_1}{F_2 - F_1}$ and $0.001 < m < 0.002$. This relation is correct to within 2 percent. If α_{o_e}' is also assumed to be approximately equal to $\left[\alpha_m - \left(\frac{d\alpha}{dF}\right)_m m\right]_e$ then

$$\alpha_{o_e} = \alpha_{o_e}' \frac{\alpha_{o_t}}{\alpha_{o_t}'}$$

$$\approx \left[\alpha_m - \left(\frac{d\alpha}{dF}\right)_m m\right]_e \frac{\left[\alpha_m - \left(\frac{d\alpha}{dF}\right)_m m + \left(\frac{d^2\alpha}{dF^2}\right)_m \frac{m^2}{2!} - \left(\frac{d^3\alpha}{dF^3}\right)_m \frac{m^3}{3!} + \cdots\right]_t}{\left[\alpha_m - \left(\frac{d\alpha}{dF}\right)_m m\right]_t}$$

$$\approx \left[\alpha_m - \left(\frac{d\alpha}{dF}\right)_m m\right]_e + \frac{\alpha_{o_e}'}{\alpha_{o_t}'}\left[\left(\frac{d^2\alpha}{dF^2}\right)_m \frac{m^2}{2!} - \left(\frac{d^3\alpha}{dF^3}\right)_m \frac{m^3}{3!} + \cdots\right]_t$$

In words, the extrapolated experimental value, α_{o_e}, is approximately equal to the experimental linear extrapolation from $F = m$ plus a slightly modified theoretical curvature correction.

REFERENCES

1. Eckert, E. R. G., and Livingood, John N.: Comparison of Effectiveness of Convection-, Transpiration-, and Film-Cooling Methods With Air as Coolant. NACA TN 3010, 1953.

2. Eckert, E. R. G.: Heat Transfer and Temperature Profiles in Laminar Boundary Layers on a Sweat-Cooled Wall. TR 5646, Army Air Forces, Air Materiel Command, Wright Field, Dayton, Ohio, Nov. 3, 1947.

3. Brown, W. Byron, and Donoughe, Patrick L.: Tables of Exact Laminar-Boundary-Layer Solutions When the Wall is Porous and Fluid Properties are Variable. NACA TN 2479, 1951.

4. Low, George M.: The Compressible Laminar Boundary Layer With Fluid Injection. NACA TN 3404, 1955.

5. Dorrance, William H., and Dore, Frank J.: The Effect of Mass Transfer on the Compressible Turbulent Boundary-Layer Skin Friction and Heat Transfer. Jour. Aero. Sci., vol. 21, no. 6, June 1954, pp. 404-410.

6. Rubesin, Morris W.: An Analytical Estimation of the Effect of Transpiration Cooling on the Heat-Transfer and Skin-Friction Characteristics of a Compressible, Turbulent Boundary Layer. NACA TN 3341, 1954.

7. Mickley, H. S., Ross, R. C., Squyers, A. L., and Stewart, W. E.: Heat, Mass, and Momentum Transfer for Flow Over a Flat Plate With Blowing or Suction. NACA TN 3208, 1954.

8. Chauvin, Leo T., and Carter, Howard S.: Exploratory Tests of Transpiration Cooling on a Porous 8° Cone at $M = 2.05$ Using Nitrogen Gas, Helium Gas, and Water as the Coolants. NACA RM L55C29, 1955.

9. Rubesin, Morris W.: A Review of Recent Advances in Knowledge of Heat Transfer and Skin Friction in High-Speed Aerodynamics. NACA Univ. Conf. on Aerodynamics, Construction, and Propulsion. Vol. II - Aerodynamics. Lewis Flight Propulsion Lab., Cleveland, Ohio, Oct. 20-22, 1954, paper 14, pp. 1-15.

10. Stalder, Jackson R., Rubesin, Morris W., and Tendeland, Thorval: A Determination of the Laminar-, Transitional-, and Turbulent-Boundary-Layer Temperature-Recovery Factors on a Flat Plate in Supersonic Flow. NACA TN 2077, 1950.

11. Dannenberg, Robert E., Weiberg, James A., and Gambucci, Bruno J.: The Resistance to Air Flow of Porous Materials Suitable for Boundary-Layer-Control Applications Using Area Suction. NACA TN 3094, 1954.

12. Rubesin, Morris W.: The Effect of an Arbitrary Surface-Temperature Variation Along a Flat Plate on the Convective Heat Transfer in an Incompressible Turbulent Boundary Layer. NACA TN 2345, 1951.

13. Pappas, C. C.: Measurement of Heat Transfer in the Turbulent Boundary Layer on a Flat Plate in Supersonic Flow and Comparison with Skin-Friction Results. NACA TN 3222, 1954.

14. Grootenhuis, P., and Moore, N. P. W.: Some Observations on the Mechanism of Sweat Cooling. Proc. of 7th International Congress for Appl. Mechanics, vol. 3, 1948, pp. 106-119.

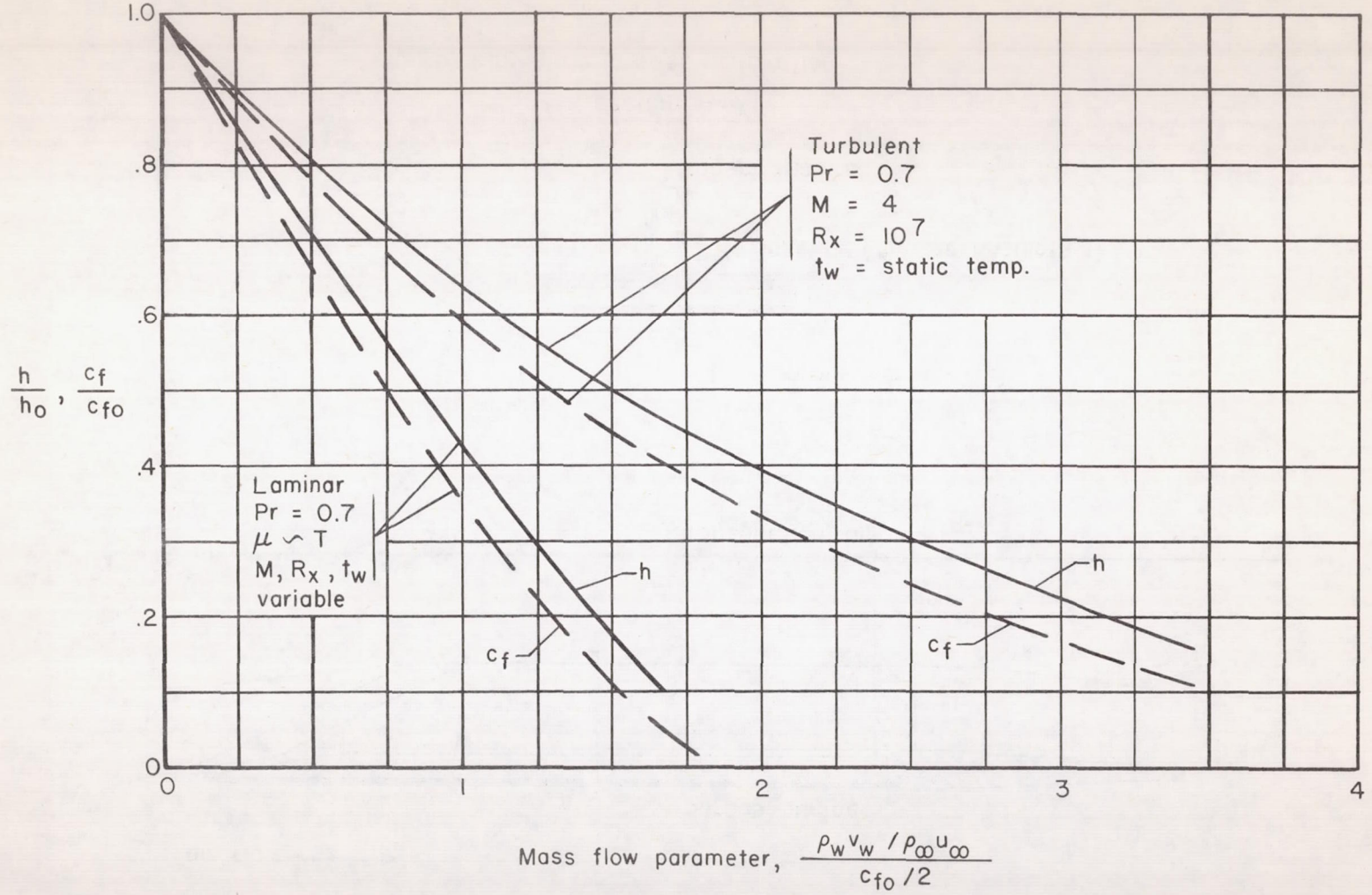

Figure 1.- Effect of transpiration on heat transfer and skin friction in a boundary layer on a flat plate (ref. 9).

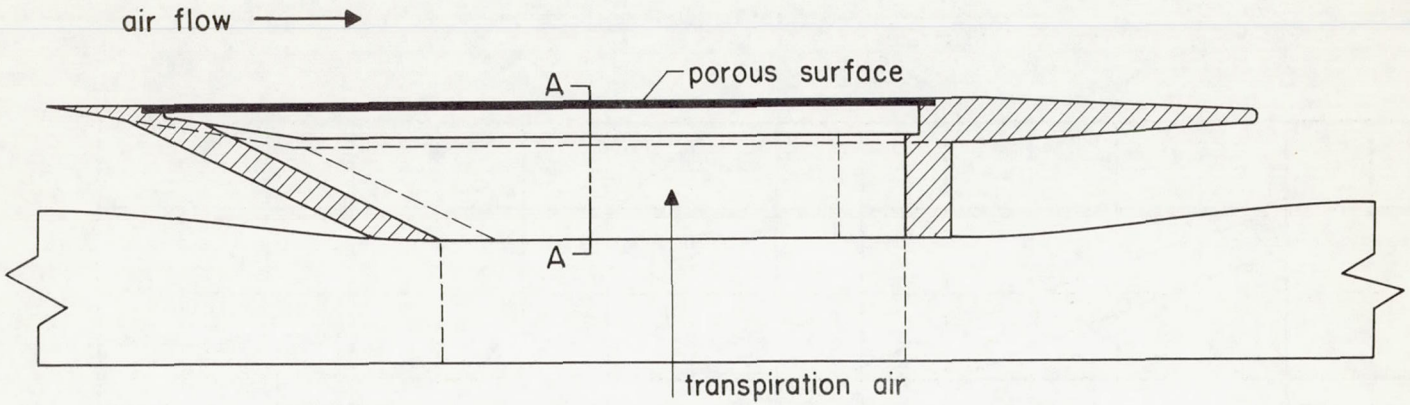

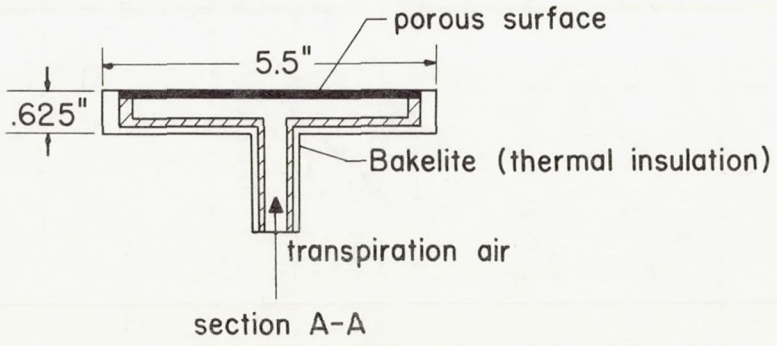

(a) Flat-plate model installation

Figure 2.- Schematic drawing of model construction.

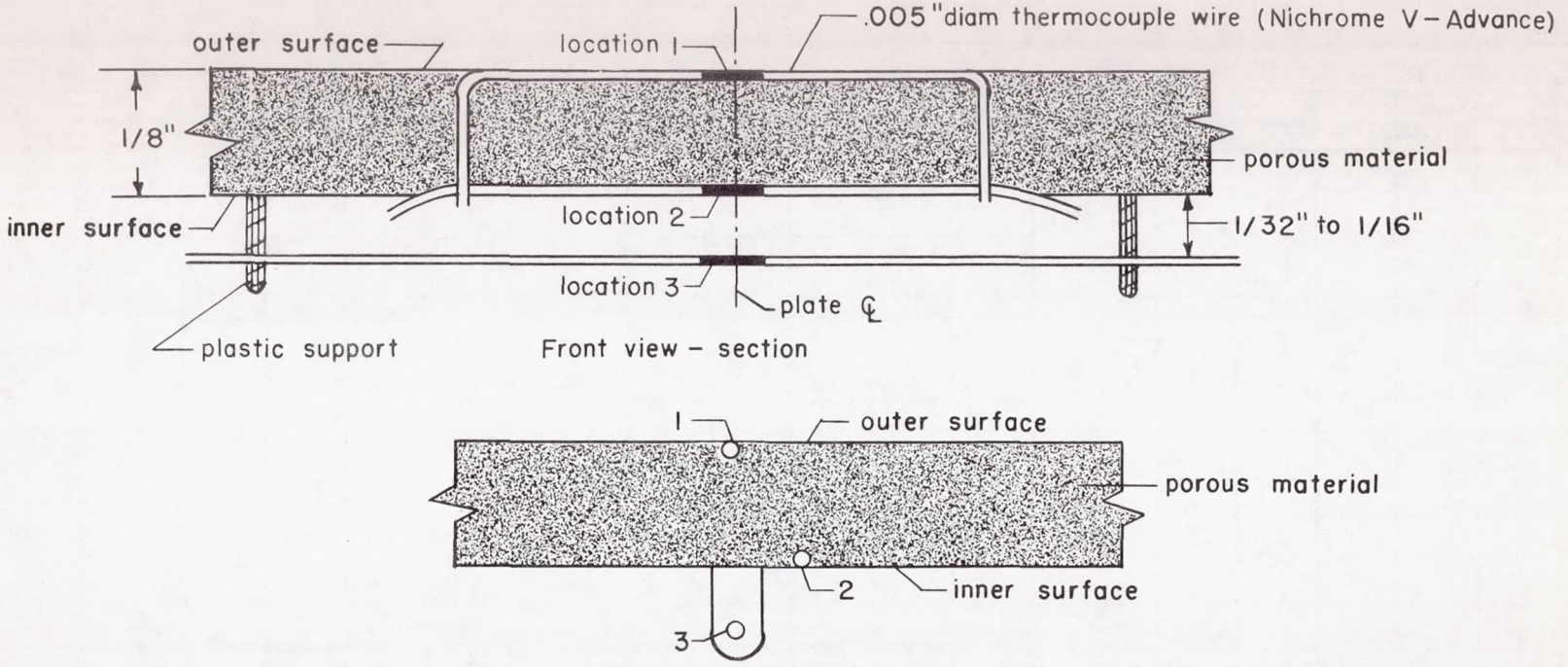

(b) Thermocouple installation and location.

Figure 2.- Concluded.

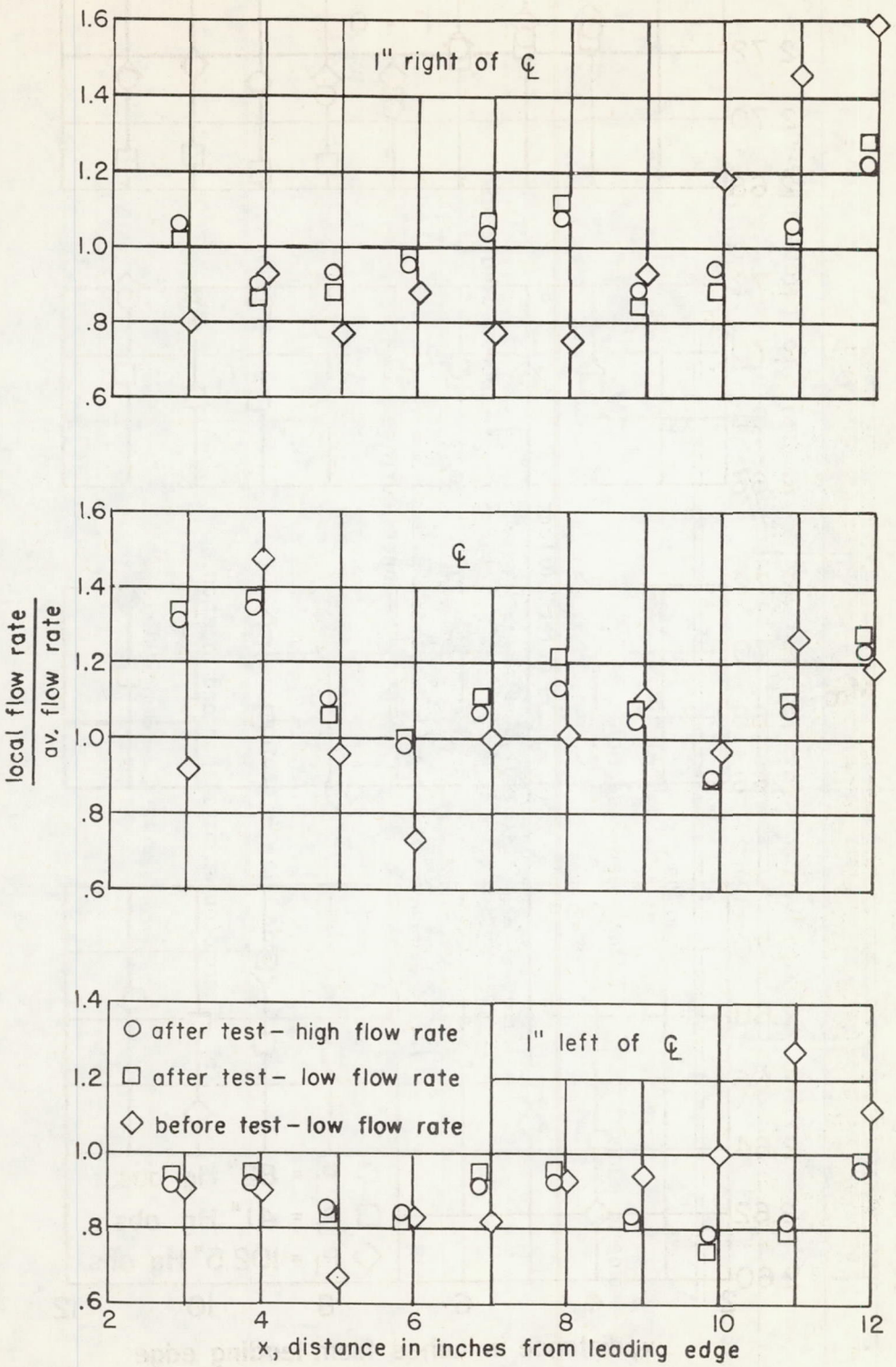

Figure 3.- Relative porosity of porous flat plate.

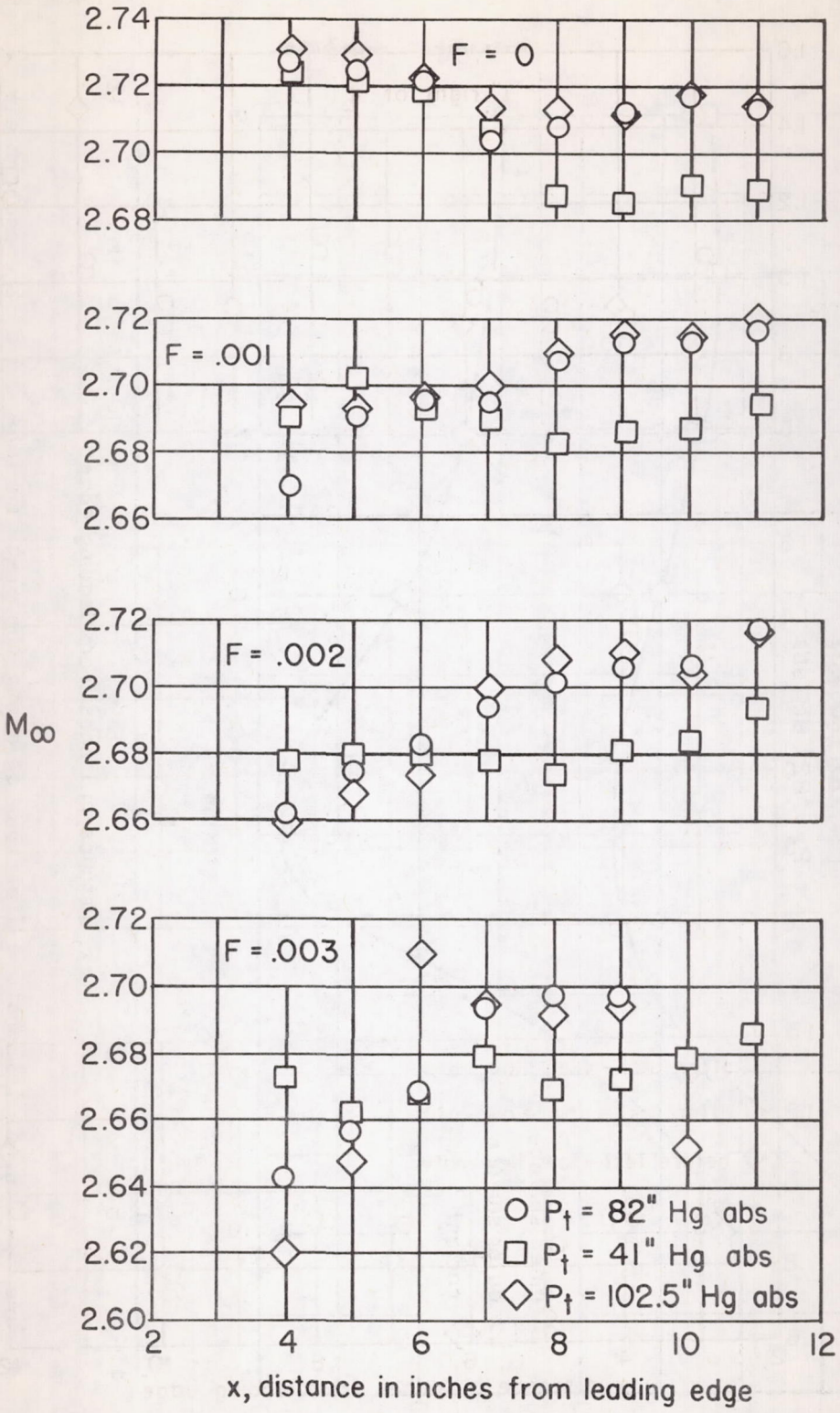

Figure 4.- Axial free-stream Mach number distributions along the flat plate.

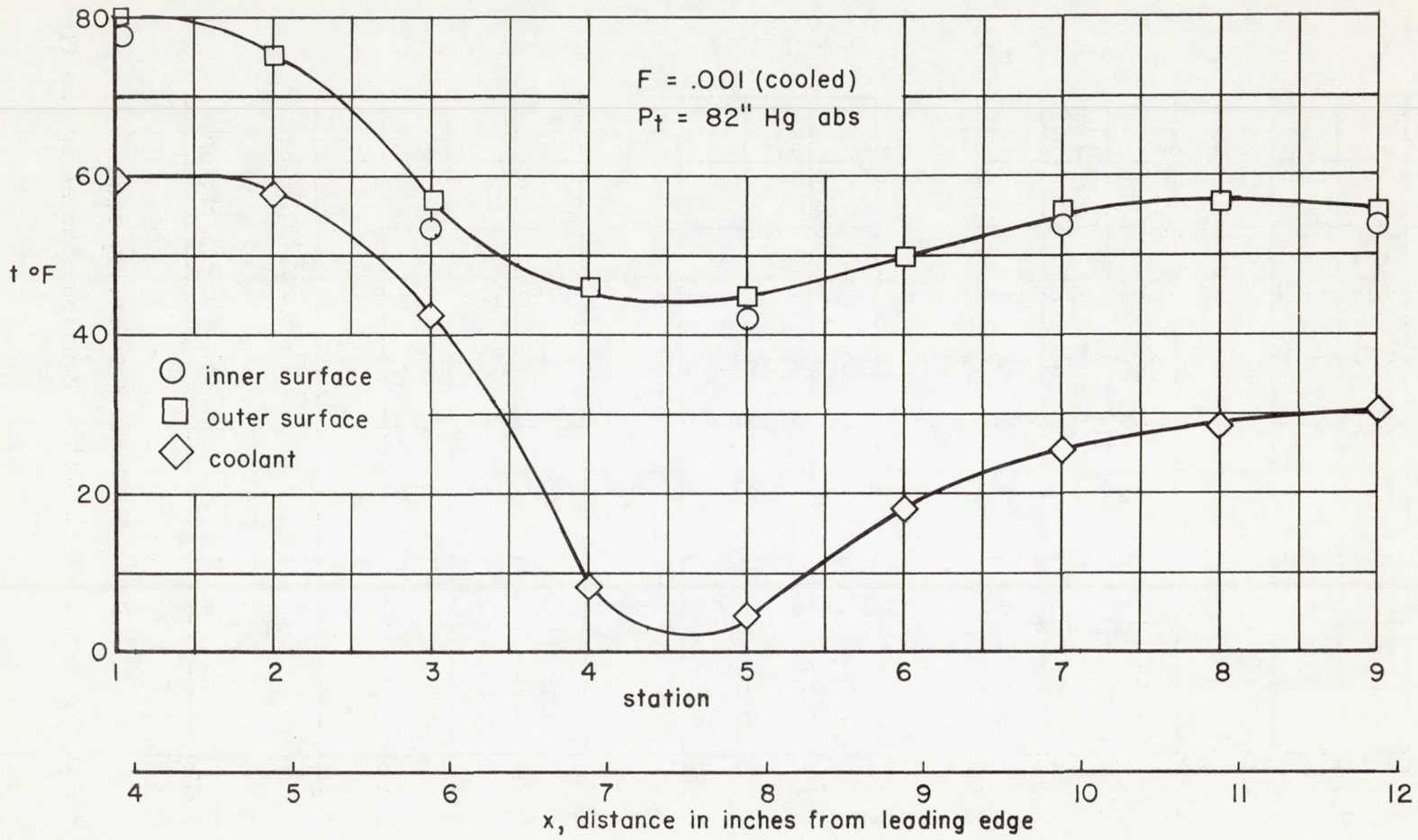

Figure 5.- Typical temperature distribution along the plate surface and of the coolant air beneath the surface.

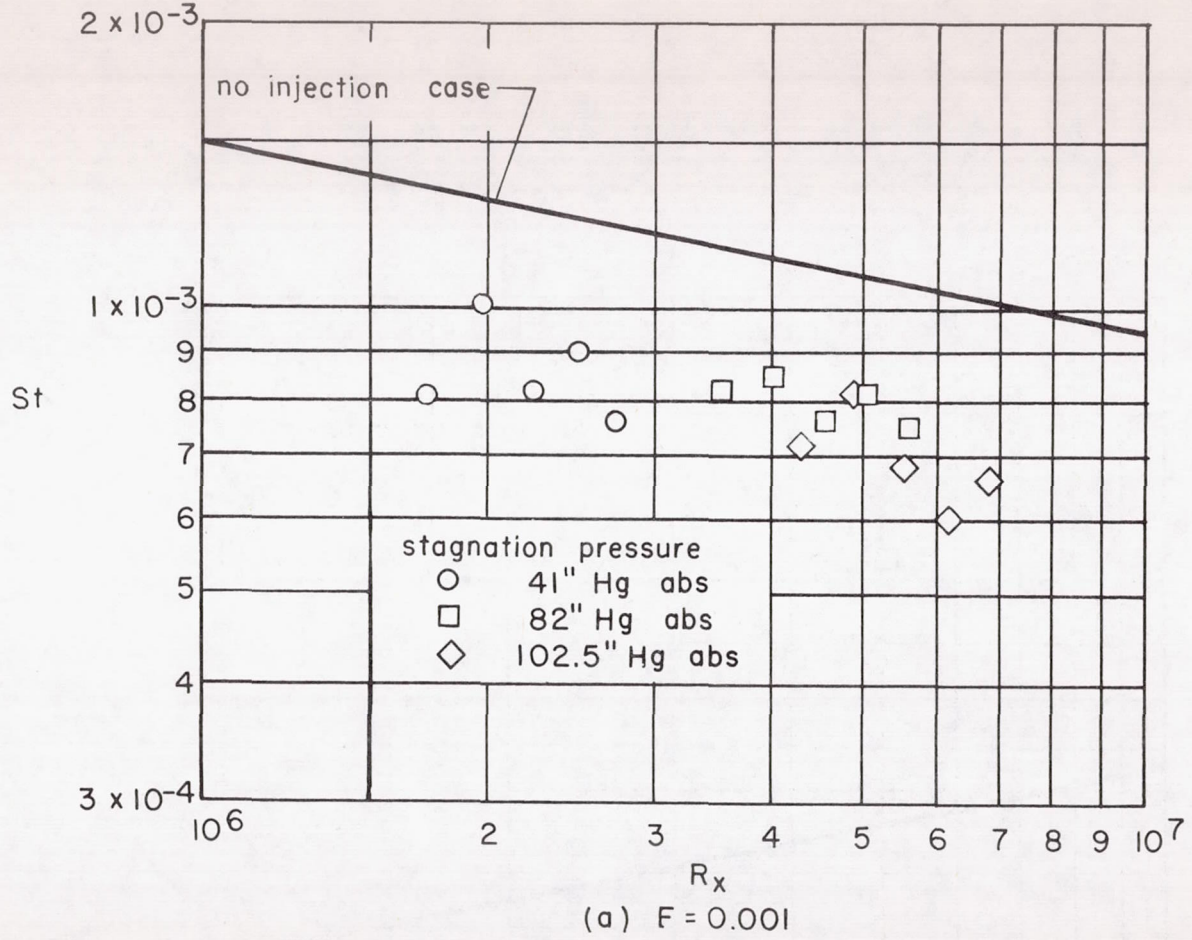

Figure 6.- Effect of transpiration rate on the relation between local Stanton number and length Reynolds number. (Line represents Colburn incompressible equation corrected to Mach number 2.7 by $t_w = t_r$ curve in ref. 13.)

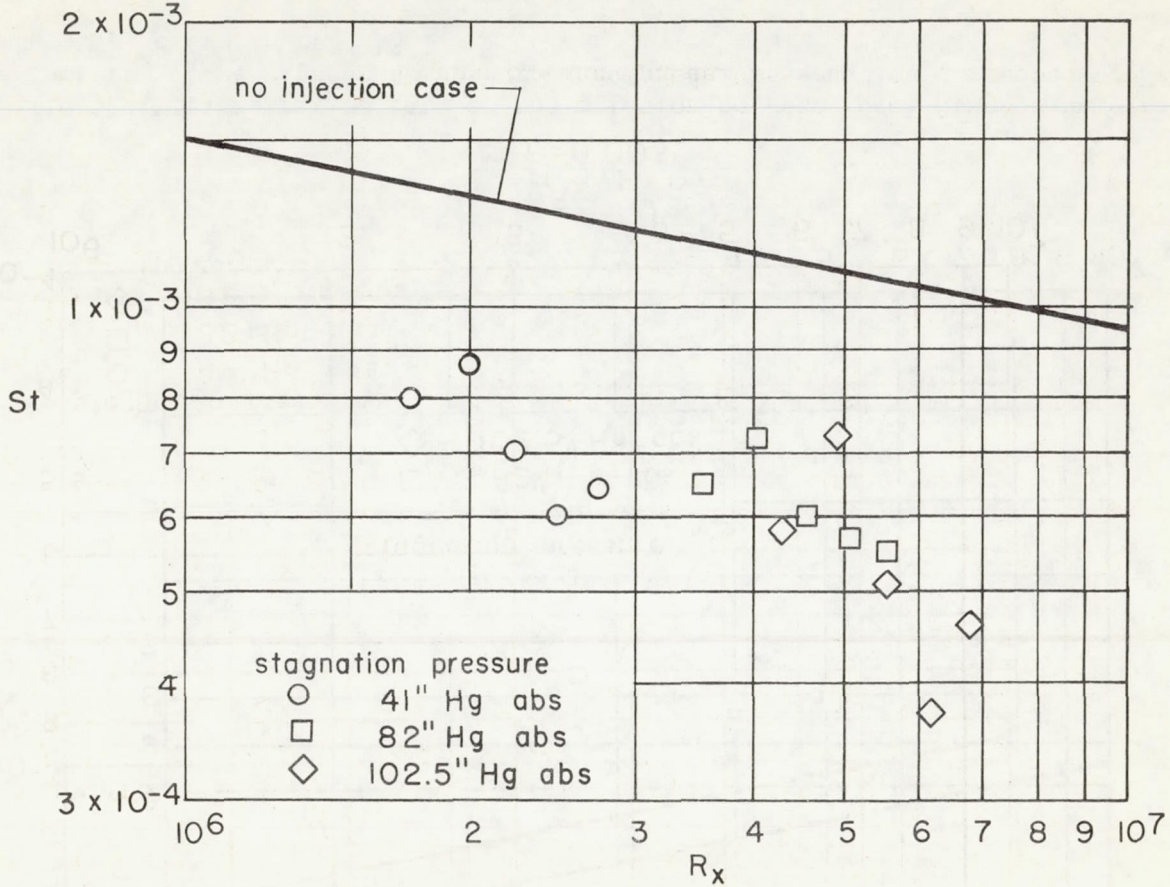

(b) F = 0.002

Figure 6.- Continued.

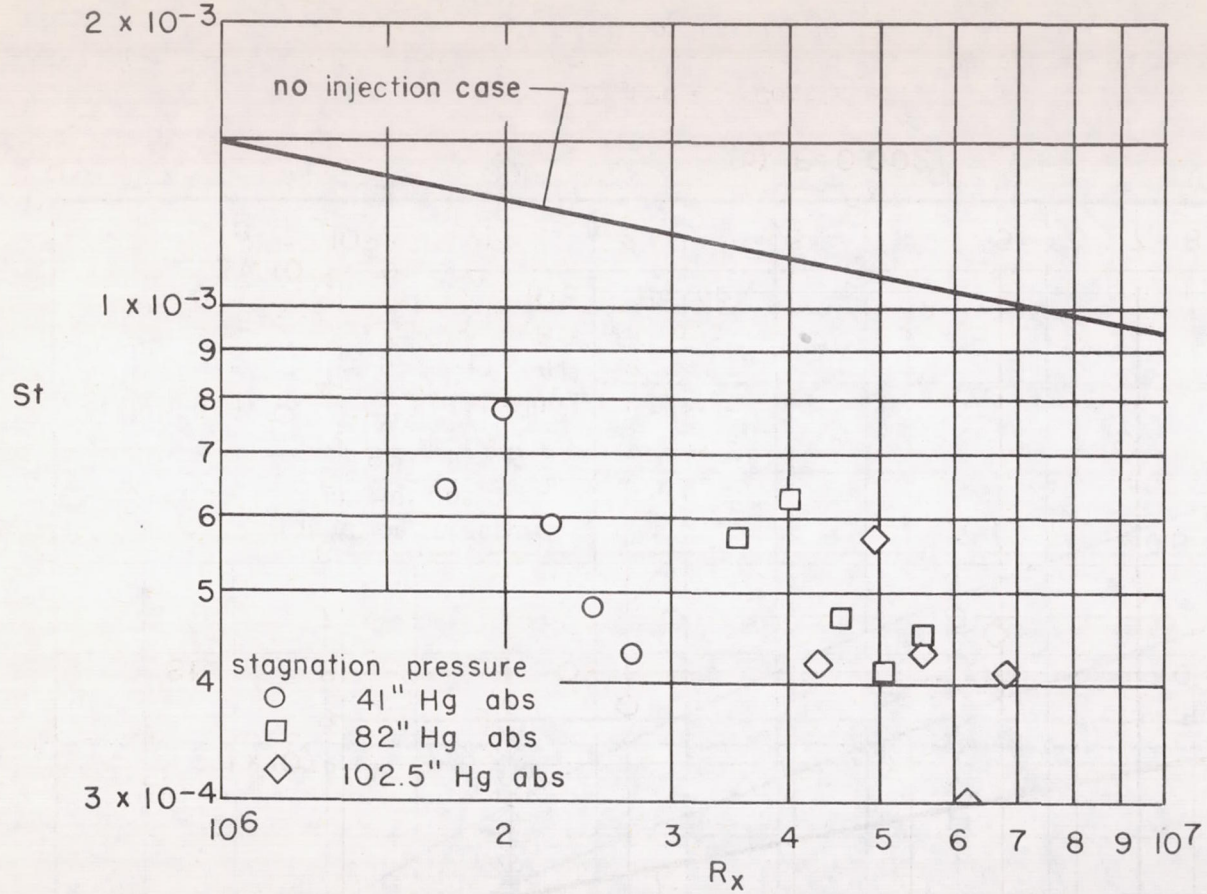

(c) F = 0.003

Figure 6.- Concluded.

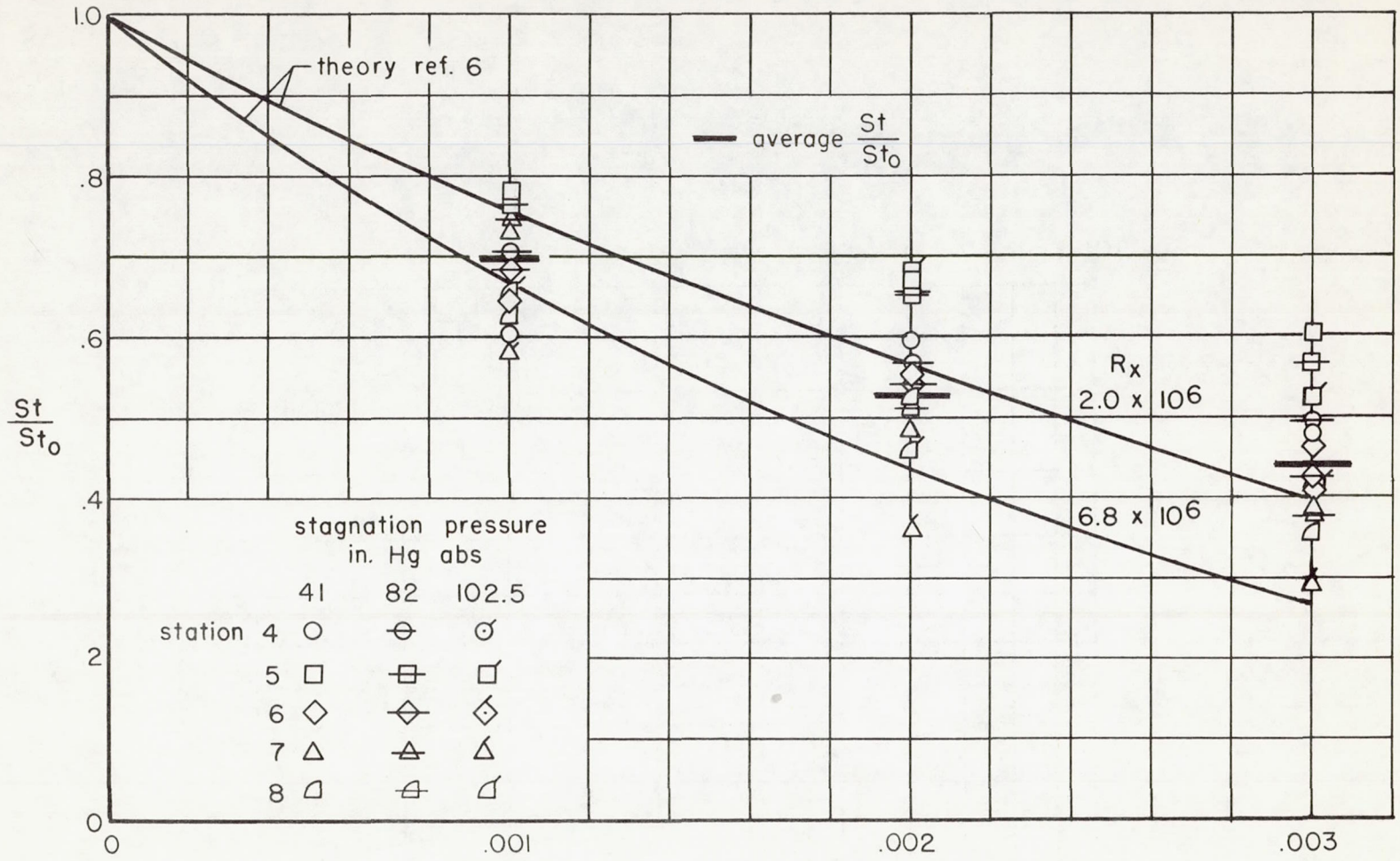

Figure 7.- Variation of ratio of local Stanton number with transpiration rate; St_o based on data of reference 13.

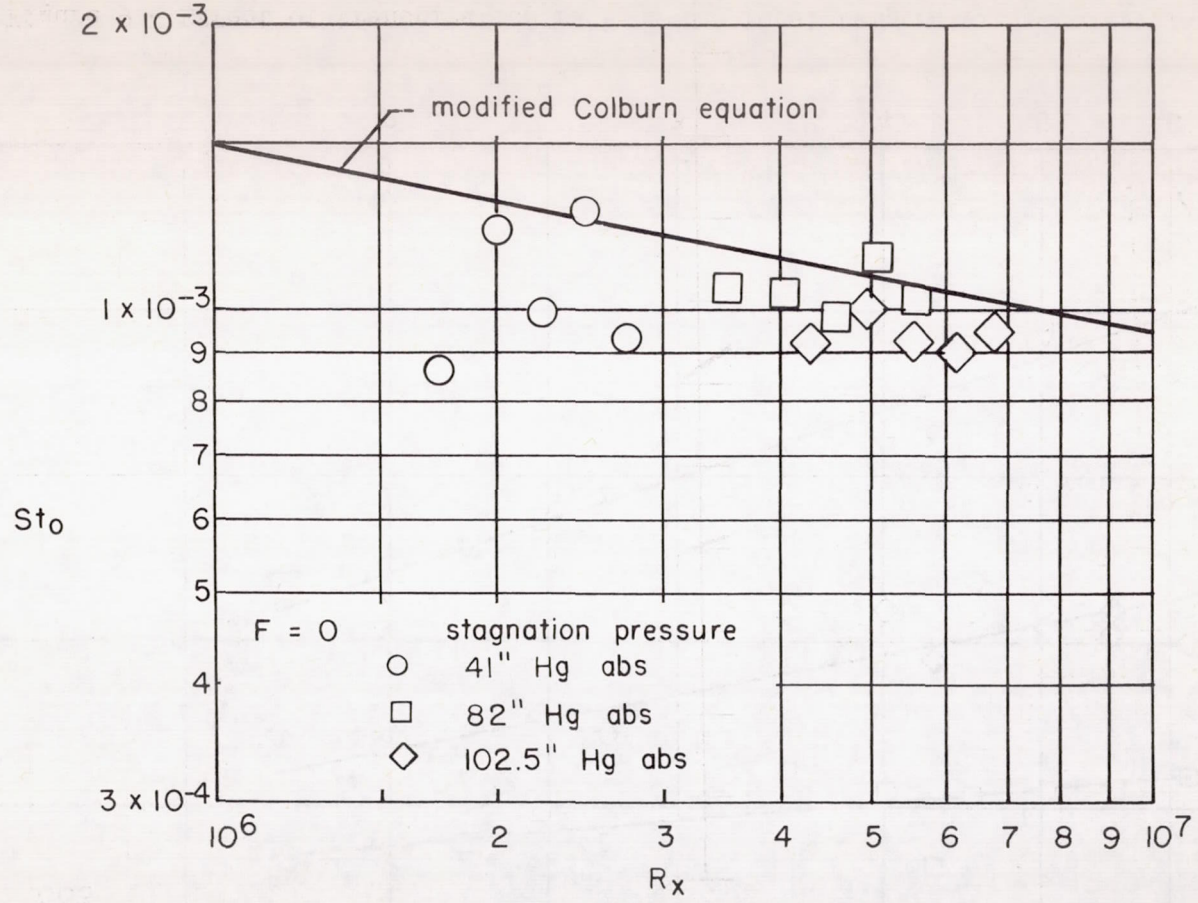

Figure 8.- Comparison of local Stanton numbers extrapolated to zero transpiration with modified Colburn equation.

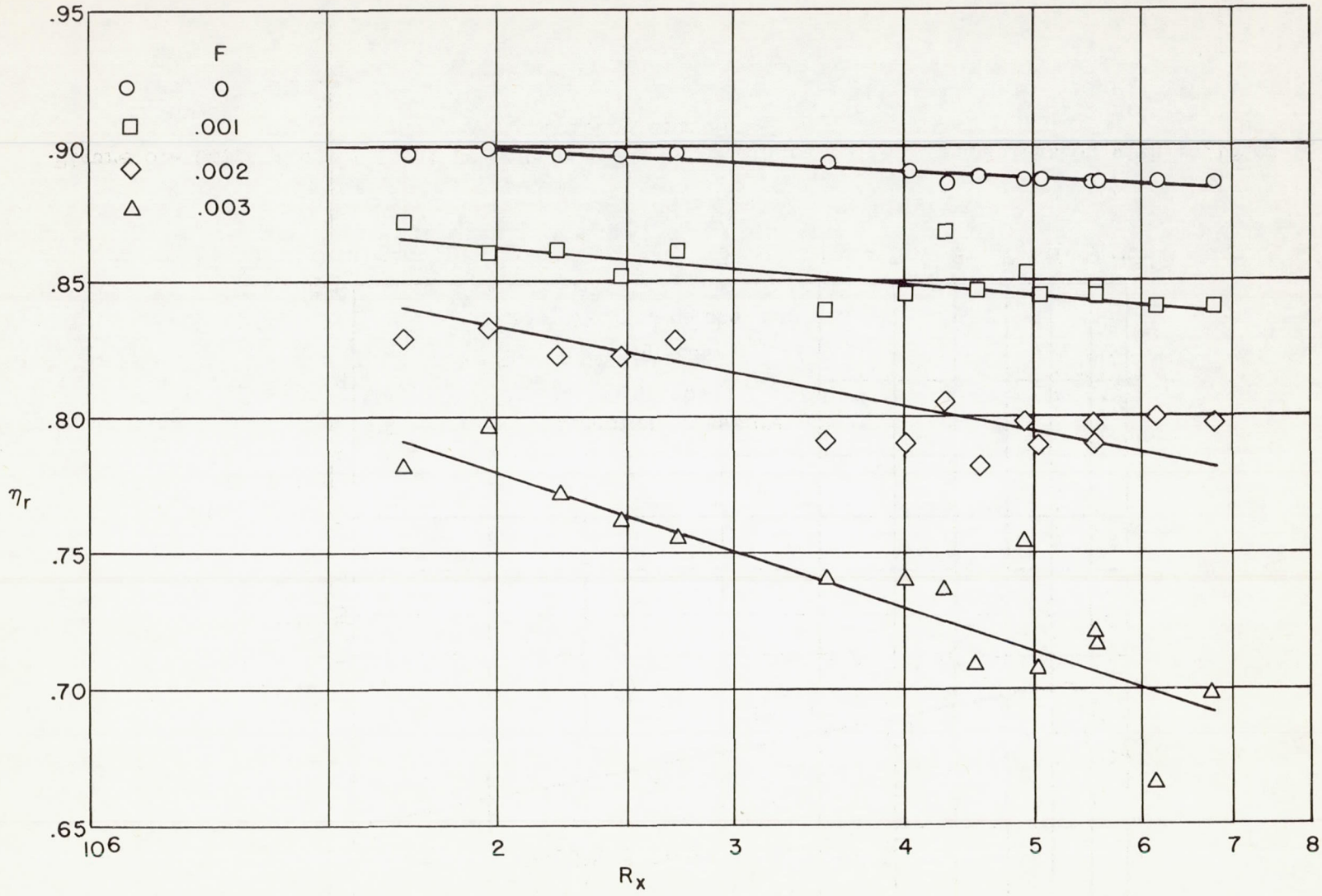

Figure 9.- Effect of transpiration rate on the local temperature recovery factor.

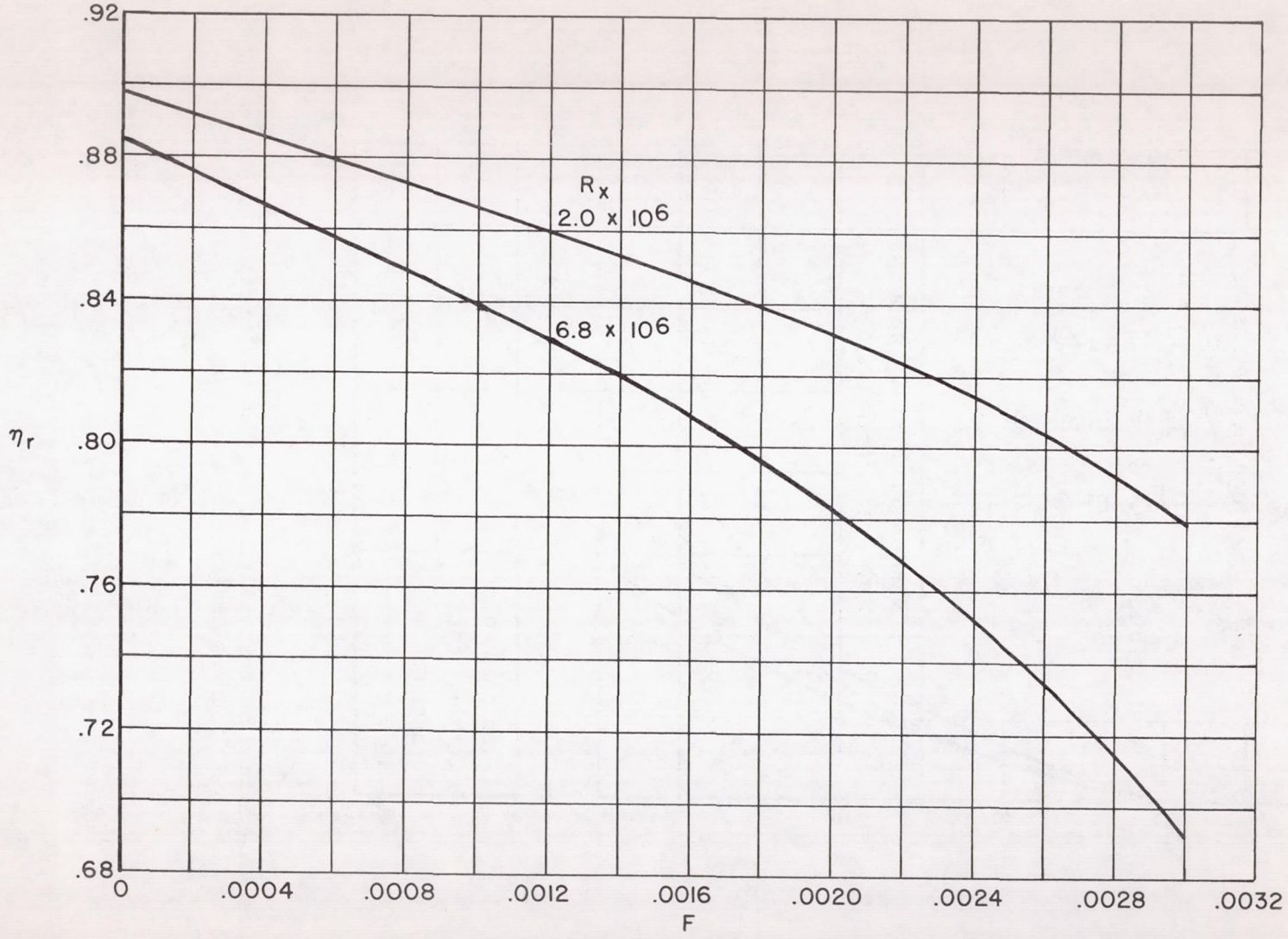

Figure 10.- Variation of temperature recovery factor with transpiration rate.

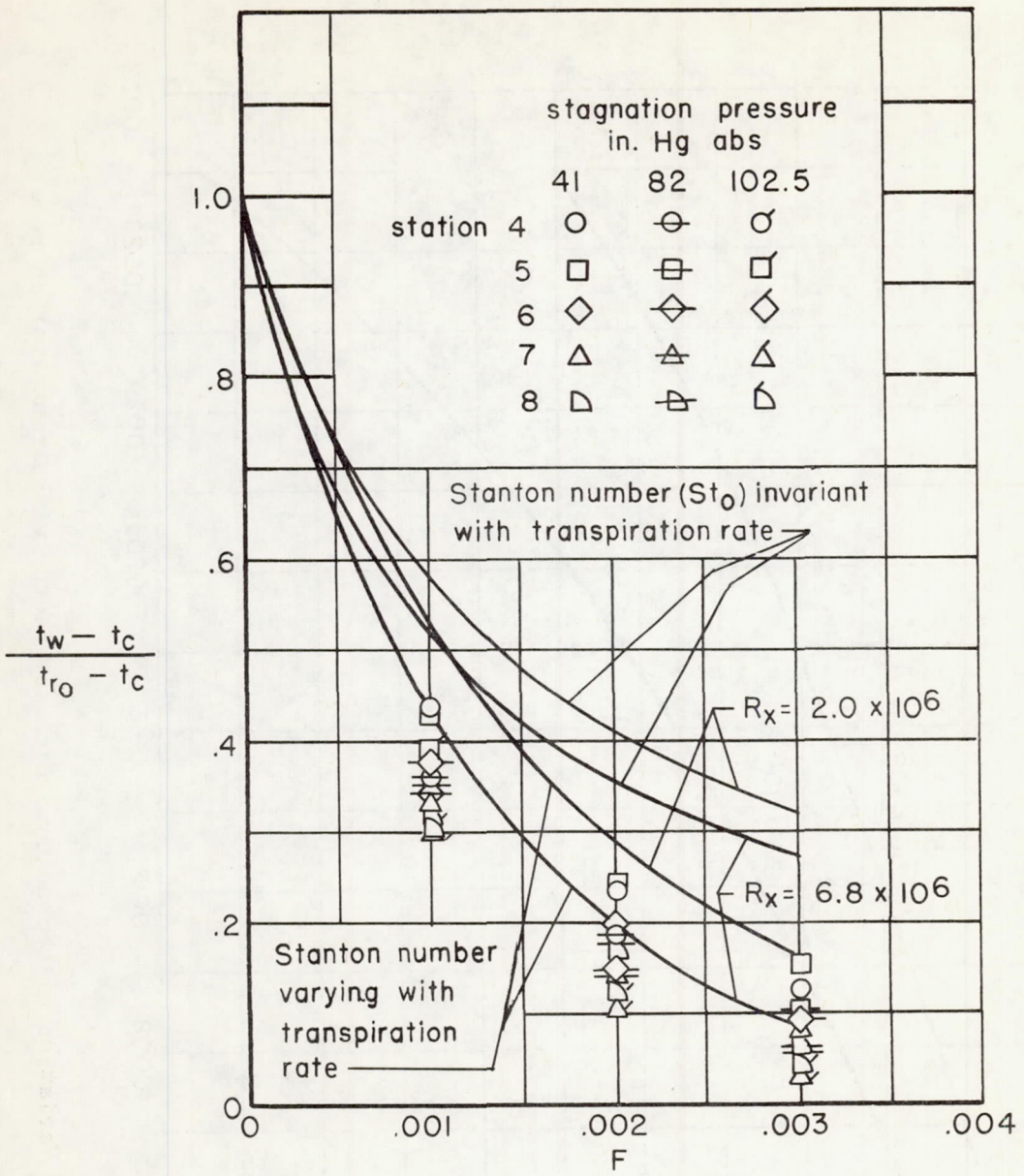

Figure 11.- Effect of transpiration rate on wall temperature parameter (curves determined using ref. 6).

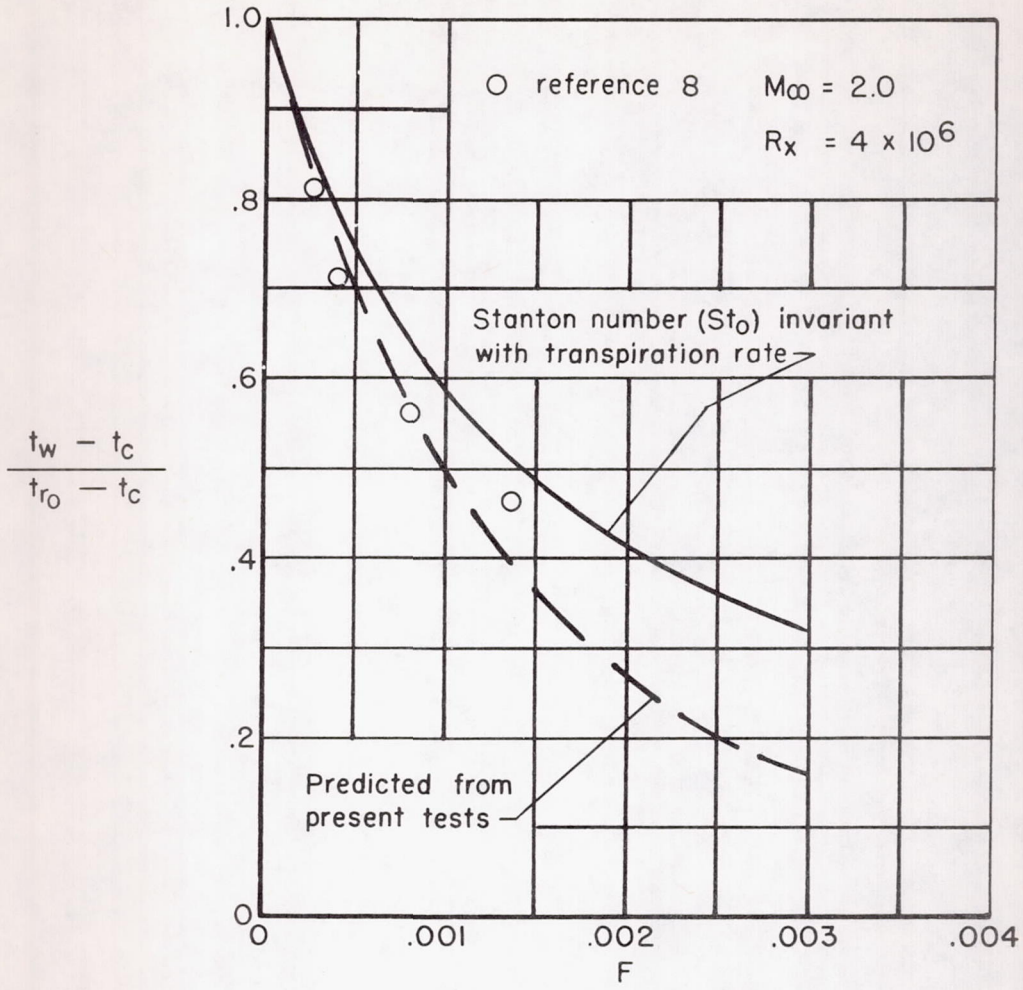

Figure 12.- Comparison of data of reference 8 with predicted wall temperature parameter based on present test results.